

Effect of Synchronisation Error on Optical Spatial Modulation

Hammed G. Olanrewaju, and Wasu O. Popoola, *Senior Member, IEEE*

Abstract—This work examines the effect of synchronisation error on the performance of spatial modulation (SM) technique in optical wireless communication (OWC) systems. SM exploits the deployment of multiple transmitters by encoding user information on their spatial domain. In most works related to SM, a perfect synchronisation among these multiple transmitters is assumed. However, synchronisation error can result from multipath propagation in OWC channel, and clock jitter and variation in propagation delay of each transmitter. Such error in synchronisation degrades system performance and hence the need to investigate its effect. Using union bound technique, and defining synchronisation errors as timing offsets in the received signals, we derive the symbol error rate for space shift keying (SSK), generalised SSK (GSSK), SM and generalised SM (GSM) schemes, and we validate our analysis with tightly-matched simulation results. Results show degradation in performance increases with synchronisation error. While SSK is tolerant for a small range of synchronisation error, GSSK, SM and GSM are significantly impaired. Our results also demonstrate the dependence of SM on channel gain values. We observe that the lower the channel gain of the transmitter in which synchronisation error occurs, the lesser the impact of the synchronisation error on the system performance.

Index Terms—Optical communication, visible light communications, multiple-input-multiple-output (MIMO) systems, spatial modulation, synchronisation, digital modulation.

I. INTRODUCTION

MULTIPLE-input-multiple-output (MIMO) systems constitute a key technology in improving the capacity and/or reliability of wireless communications. However, such improved system performance comes at the cost of increase in system complexity and cost [1]. Spatial modulation (SM) has been extensively studied as a promising MIMO technique which promotes lower system complexity, and has the potential to support high data-rate and energy-efficient wireless communication [2]–[8].

As a MIMO technique, SM requires the deployment of multiple transmit elements, exploiting their spatial domain to convey all or some of the information bits of the transmitted symbol. SM has been implemented in a variety of forms, using different modulation methods, and activating single or multiple transmit elements. For instance, space shift keying (SSK) [4] is a subset of SM which entails activating only one transmitter in any symbol duration, and encoding the information bits solely on the spatial index of the activated transmitter. Other forms of SM entail encoding some information bits in the indices of the transmitters while the rest of the information

bits are conveyed by the transmitted signal modulation such as pulse position modulation (PPM) [7], pulse amplitude modulation [2], quadrature amplitude modulation (QAM) [9] and orthogonal frequency division multiplexing (OFDM) [10], [11]. An example of such schemes is the spatial pulse position modulation (SPPM) scheme [7] which combines SSK and PPM. Additionally, generalised SM schemes have been developed to activate multiple transmit elements concurrently, thereby increasing the system capacity [12]–[15]. A detailed comparison of optical SM with other MIMO techniques has been studied in literature including [2], [16], [17].

Timing synchronisation plays an important role in MIMO systems [18], [19]. Imperfect timing synchronisation causes the receiver to read a mixture of interfering signals at its sampling instant. These interfering signals constitute intersymbol interference (ISI) in the transmitted data streams. This compromises the transmitted symbol, resulting in increased error rate. Hence, synchronisation problems, including performance analysis, timing estimation, and correction, must be addressed in order to avoid performance degradation in practical networks. Errors in timing synchronisation in optical MIMO system can occur due to clock jitter in the transmitters, multipath propagation in optical wireless channel [20]–[22], and the differences in propagation delays due to the spatial separation of the transmit units (Light emitting diodes (LEDs)) and the receiver mobility.

Timing synchronisation is especially important for MIMO systems with significant physical separation between the multiple elements at the transmitter and the receiver side. For instance, in cooperative MIMO systems in which the antennas are physically separated, timing synchronisation is a major issue, and this has been investigated in literature including [23] and [24]. As established in previous reports on SM, the performance of SM technique is highly dependent on the dissimilarity of the channel gains of the transmit-receive paths [1], [2], [25]. However, the optical MIMO channel can be highly correlated if the locations of the transmit and receive units are not optimized [26], [27], which results in a significant penalty in error performance. By physically separating the MIMO transmit-receive paths in order to achieve channel gain dissimilarity, each path may experience slightly different propagation characteristics such as channel delay. This causes multiple timing offsets between the transmitter and the receiver. A similar variation in channel characteristics is expected if the receiver is moved from one point to another. Consequently, in optical SM schemes, even though the LEDs are not activated concurrently, synchronisation error can occur if the signal transmitted by each LED experiences different

The authors are with the Institute for Digital Communications and the LiFi R&D, School of Engineering, University of Edinburgh, UK. e-mail: {g.olanrewaju and w.popoola}@ed.ac.uk.

channel delay. In the case of generalised optical SM schemes, timing synchronisation is even more essential since multiple LEDs transmit data signals concurrently [13].

Moreover, since additional information bits are encoded in the signal transmitted by the activated LED(s) in SM techniques, the sensitivity of the employed signal modulation to synchronisation issues is also very relevant. The effect of synchronisation error on the modulating signal constellations that are widely used for optical communication has previously been studied in [28]–[32]. The theoretical analysis of the effect of synchronisation error on-off keying and PPM are presented in [28]. Similarly, an inverse pulse position modulation (IPPM) method is proposed for visible light communication in [29], and models are derived show the effect of clock time shift and jitter on the error performance. In [30], a coding theoretic framework is proposed to address the synchronisation issues of pulse position based signal modulation techniques. References [31] and [32] studied the impact of imperfect synchronisation on optical OFDM systems and they present techniques to mitigate its effect.

In most research works related to SM, it is assumed that timing is perfectly synchronised among the multiple transmit and receive units in the SM scheme. That is, the signals received from the transmit units have the same clock timing, and they experience the same propagation delay. However, the aforementioned factors have motivated the need to examine this assumption and to analyse the effect of timing synchronisation error on the performance of optical SM schemes. In this paper, we consider the effect of synchronisation error on optical SM techniques involving both the spatial and the signal constellations. To the best of our knowledge, this has not been reported in literature. Specifically, by utilising the union bound technique [33], and defining synchronisation error as timing offset in the received signal, we derive the analytical upper bound on the symbol error rate (SER) of optical SSK (OSSK), generalised SSK (GSSK), optical SM and generalised optical SM (GSM) schemes, under the condition of imperfect synchronisation. Furthermore, simulations are performed to validate the results of the theoretical analyses. Without loss of generality, SPPM [7] is used as a case study for optical SM techniques, while generalised SPPM (GSPPM) [15] is considered as a case study for GSM.

The rest of this paper is organised as follows: the description of the four optical SM schemes studied in this paper is presented in Section II. Using GSPPM as a reference scheme, Section III provides a general system model for optical SM schemes, and in Section IV, the theoretical analysis of the effects timing error on the performance of GSPPM-based OWC systems is presented. The analysis of the effect of timing error on GSPPM is extended to OSSK, GSSK, and SPPM in Section V. Section VI provides the analytical and simulation results of the performance evaluation of the four schemes and concluding remarks are given in Section VII.

II. DESCRIPTION OF OSM SCHEMES

IN this section, we provide a brief description of the four variants of optical SM studied in this work. As mentioned

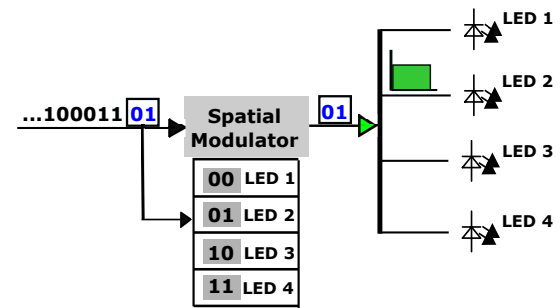


Fig. 1: An illustration of OSSK modulation using $N_t = 4$ LEDs.

in Section I, the differences in these variants include, but not limited to, the number of LEDs that are activated concurrently, and whether or not digital signal modulation is transmitted by the activated LEDs. Considering an optical MIMO system with N_t LEDs, at the transmitter, the information bits to be transmitted are grouped into data symbols, and the bits that make up each data symbol are grouped into two: spatial bits and signal bits. The spatial bits make up the spatial constellation point (SCP) which determines the indices (position) of the LEDs that will be activated, while the signal bits constitute the signal constellation point that determines the electrical signal modulating the intensity emitted by the activated LEDs. Let the spatial and signal constellation sizes be denoted by K and L respectively, there are $(K \times L)$ possible data symbols and the number of bits transmitted per symbol is given by $M = \log_2(KL)$.

A. Optical space shift keying (OSSK)

In OSSK, only one LED is activated to send an optical data signal during a given symbol duration, while the rest of the LEDs are idle. However, the activated LED does not transmit any digital signal modulation. Therefore, the data symbol is encoded solely in the SCP, i.e., the index of the activated LED. The activated LED transmits a rectangular optical pulse of constant peak power, P_t , for the entire symbol duration T . With a total of N_t LEDs, $K = N_t$, and since no signal modulation is used, $L = 1$. Hence, a total of $M = \log_2(N_t)$ bits are transmitted per symbol. An illustration of OSSK modulation scheme with 4 LEDs is depicted in Fig. 1. Two information bits are transmitted per symbol, and the first two bits, ‘01’, are transmitted by activating ‘LED 2’. The achieved transmission rate in OSSK can be increased by adding signal modulation and/or activating multiple LEDs concurrently, as employed in the SM schemes discussed next.

B. Generalised space shift keying (GSSK)

Unlike SSK in which only one LED is activated in any given symbol duration, in optical GSSK [8], [12], one or more LEDs can be activated concurrently. However, signal modulation is not used in GSSK too, i.e., $L = 1$. Hence, the data symbol is encoded solely in the SCP. Using N_t LEDs, $K = 2^{N_t}$, and $M = N_t$ bits/symbol. As described in [8], the number and the position of ones (1s) in the bit make-up of each symbol determine the number and the indices of the LEDs that will be activated to convey the symbol. For any given data symbol,

Data symbol	Binary equivalent	LED 1	LED 2
0	00		
1	01	IDLE	
2	10		IDLE
3	11		

Fig. 2: An illustration of the pulse pattern for optical GSSK scheme with $N_t = 2$ LEDs.

except when all the bits are zeros, the LEDs whose positions correspond to a bit value of one are activated to transmit a return-to-zero (RZ) pulse with duty cycle δ and peak power P_t , while all the other LEDs are idle, where $0 < \delta \leq 1$. However, when the bits of the symbol are all zeros, all the LEDs are activated, but they transmit a pulse with duty cycle $(1 - \delta)$. As an illustration, the pulse pattern for a 2-LED GSSK scheme is shown in Fig. 2.

C. Spatial pulse position modulation (SPPM)

As in OSSK, only one of the N_t LEDs is activated during a given symbol duration in SPPM scheme. However, unlike OSSK, signal modulation is employed to transmit additional information bits in SPPM. The activated LED transmits an L -PPM optical signal rather than a constant optical power for the entire symbol duration [7], where L is the number of PPM time slots in a symbol period, and hence it is the signal constellation size. In SPPM, $K = N_t$ and total number of bits transmitted per symbol is $M = \log_2(LN_t)$. At the transmitter, the first $\log_2(N_t)$ most significant bits of each data symbol constitute the spatial bits, while the remaining $\log_2(L)$ bits constitute the signal bits which determine the pulse position of the PPM signal transmitted by the activated LED. The SPPM scheme is illustrated in Fig. 3 for the case of $N_t = 4$, $L = 2$ and $M = 3$ bits/symbol. As an example, symbol '3' with binary representation '011', is transmitted by activating 'LED 2' to transmit a pulse in the second time slot.

D. Generalised spatial pulse position modulation (GSPPM)

In a GSPPM scheme, one or more LEDs can be activated to concurrently transmit data signals [15], and the activated LEDs transmit the same L -PPM pulse pattern in a similar fashion to SPPM. The spatial constellation size, $K = 2^{N_t}$, and that of the signal constellation is L . Therefore, $M = N_t + \log_2(L)$. The most significant N_t bits of each symbol constitute the spatial bits, while the remaining $(\log_2 L)$ bits constitute the signal bits which is conveyed by the pulse position of the PPM signal transmitted by activated LEDs. LED activation in GSPPM [15] is done in a similar way to the GSSK scheme, albeit with a slight modification. That is, the number of ones (1s) in the spatial bits still determines the number and the indices of the

Data symbol	Binary equivalent	Activated source	Sample PPM pulse pattern
0	000	LED 1	[000]
1	001		
2	010	LED 2	[011]
3	011		
4	100	LED 3	[100]
5	101		
6	110	LED 4	[111]
7	111		

Fig. 3: An illustration of the pulse pattern for SPPM scheme with $N_t = 4$, $L = 2$ and $M = 3$ bits/symbol. The sample PPM patterns represent the pulse pattern for the data bits indicated in the square brackets.

Data symbol	Binary equivalent	Spatial Constellation	Signal Constellation	Activated LEDs	Sample PPM Signal Pattern
0	000	00	0	1 and 2	[000]
1	001	00	1		[-V]
2	010	01	0	1	[011]
3	011	01	1		[V]
4	100	10	0	2	[100]
5	101	10	1		[V]
6	110	11	0	1 and 2	[111]
7	111	11	1		[V]

Fig. 4: An illustration of the pulse pattern for GSPPM scheme with $N_t = 2$, $L = 2$ and $M = 3$ bits/symbol. The sample PPM patterns represent the pulse pattern for the data bits indicated in the square brackets.

active LEDs, but a pulse-inversion technique [34] is employed in GSPPM in place of the RZ pulse coding used in GSSK. Using the pulse-inversion technique in GSPPM, when the spatial bits are all zeros, all the LEDs are activated, but they are driven by an electrical pulse signal of amplitude $-V$ volts. For all other spatial constellation points, the LEDs whose indices correspond to the bit value '1' in the spatial bits are activated, and they are driven by an electrical pulse signal of amplitude V volts. By using bipolar signal of amplitude $\pm V$ volts, GSPPM requires a DC bias of V volts to convert the bipolar signal to unipolar signal, which is then used to drive the LEDs. However, for applications in visible light communications, it is assumed that this DC bias is necessary for illumination purposes anyway. GSPPM scheme is further illustrated in Fig. 4, for the case of $N_t = 2$, $L = 2$ and $M = 3$ bits/symbol. For instance, to transmit symbol '3', with binary equivalent '011', the first two bits, '01' are used to select the 'LED 1' for activation while 'LED 2' remains idle. The last bit of the symbol, 1, indicates that the pulse will be transmitted in the second time slot.

III. SYSTEM MODEL

In this section, assuming a perfect timing synchronisation at the receiver, the general system model for the four OSM schemes described in Section II is presented. First, the GSPPM scheme is used as a reference and the process of detecting the transmitted symbol is described. Next, we show how the

system parameters can be changed to obtain the system model of the other three OSM schemes.

Considering an OWC system equipped with N_t LEDs and a single receiver, let $A_{j,m}$ denote the symbol that is transmitted by activating a number of LEDs according to SCP j , $1 \leq j \leq K$, to simultaneously transmit a pulse in the m th time slot of the PPM signal, $1 \leq m \leq L$, assuming a perfect timing synchronisation between the LEDs and the receiver, then the received electrical signal, $y(t)$, in a single symbol duration T , is given by:

$$y(t) = R\mathbf{h}\mathbf{x}_{j,m}(t) + \eta(t), \quad 0 \leq t \leq T \quad (1)$$

where R is the responsivity of the photodetector (PD) and the vector $\mathbf{h} = [h_1 \dots h_{N_t}]$ is the line-of-sight (LOS) channel gain between the LEDs and the receiver. Considering a Silicon PIN photodetector with negligible dark current [22], [35], the scalar $\eta(t)$ is the sum of the ambient light shot noise and the thermal noise in the receiver. The noise term, $\eta(t)$, can therefore be modelled as independent and identically distributed additive white Gaussian noise (AWGN) with variance $\sigma^2 = \frac{N_0}{2}$, where N_0 represents the one-sided noise power spectral density [20], [36], [37]. The $(N_t \times 1)$ -dimensional vector of transmit signals, $\mathbf{x}_{j,m}(t)$, is defined as:

$$\mathbf{x}_{j,m}(t) = \mathbf{v}_j \lambda_j \phi_m(t) \quad (2)$$

where $\mathbf{v}_j = [v_1 \dots v_{N_t}]^T$ is the LED activation vector that determines the indices of the LEDs that will be activated if the symbol to be transmitted contain SCP j . The entries of \mathbf{v}_j are binary digits, with '1's' at the indices of activated LEDs, and '0's' at the indices of idle LEDs. The notation \mathcal{T} represents the transpose operation. The pulse-inversion constant $\lambda_j = -1$ if the spatial bits are all zeros, otherwise $\lambda_j = +1$. The scalar $\phi_m(t)$ is the L -PPM waveform transmitted by the activated LEDs, with the pulse of peak power, P_t , located in time slot m . It is defined as:

$$\phi_m(t) = P_t \text{rect} \left(\frac{t - (m-1)T_c}{T_c} \right), \quad 0 \leq t \leq T \quad (3)$$

where the duration of each time slot, $T_c = T/L$, and

$$\text{rect}(x) = \begin{cases} 1; & \text{for } 0 \leq x < 1 \\ 0; & \text{elsewhere.} \end{cases} \quad (4)$$

Therefore, the expression for the received electrical signal in (1) becomes:

$$y(t) = RP_t \lambda_j \mathbf{h}\mathbf{v}_j \phi_m(t) + \eta(t), \quad 0 \leq t \leq T. \quad (5)$$

As an example, using a 2-LED set-up, the electrical signal received in the pulse position of the transmitted PPM signal is obtained as shown in Table I.

Using a matched filter (MF) receiver architecture, where the receive filter, $\alpha(t)$, is given by:

$$\alpha(t) = RP_t \text{rect} \left(\frac{t}{T_c} \right), \quad 0 \leq t \leq T_c, \quad (6)$$

the MF output in each time slot, obtained by sampling at the

TABLE I: LED Activation and received electrical signal for a 2-LED GSPPM scheme

j	Spatial bits	\mathbf{v}^T	Activated LEDs	λ	$y(t)$
1	00	[1, 1]	LEDs 1 & 2	-1	$-(h_1 + h_2)RP_t + \eta(t)$
2	01	[0, 1]	LED 1	1	$h_1 RP_t + \eta(t)$
3	10	[1, 0]	LED 2	1	$h_2 RP_t + \eta(t)$
4	11	[1, 1]	LEDs 1 & 2	1	$(h_1 + h_2)RP_t + \eta(t)$

rate $1/T_c$, is given by:

$$\mathbf{r} = \mathbf{s}_{j,m} + \mathbf{n} \quad \{r_\ell\}_{\ell=1}^L = \{s_{j,m}^\ell + n_\ell\}_{\ell=1}^L \quad (7)$$

where

$$s_{j,m}^\ell = \begin{cases} \lambda_j \mathbf{h}\mathbf{v}_j E_c; & \text{if } \ell = m \\ 0; & \text{otherwise,} \end{cases} \quad (8)$$

and $\{n_\ell\}$ are the L Gaussian noise at the output of the MF in each time slot, with variance $\sigma_n^2 = \frac{N_0}{2} E_c$. The energy per symbol $E_c = (RP_t)^2 T_c$. Based on the maximum likelihood (ML) detection criterion, the estimate of the transmitted symbol is obtained from the combination of the pulse position and the spatial constellation points which gives the minimum Euclidean distance from the received signal [7], [15]. That is, the estimate of transmitted symbol, $\hat{A}_{j,m}$, is obtained as:

$$\begin{aligned} \hat{A}_{j,\hat{m}} &= [\hat{j}, \hat{m}] = \arg \max_{j,m} p(\mathbf{r} | \mathbf{s}_{j,m}) \\ &= \arg \min_{j,m} [D(\mathbf{r}, \mathbf{s}_{j,m})], \end{aligned} \quad (9)$$

where the probability density function of \mathbf{r} conditioned on $\mathbf{s}_{j,m}$ being transmitted is expressed as:

$$p(\mathbf{r} | \mathbf{s}_{j,m}) = \frac{1}{(2\pi\sigma_n^2)^{L/2}} \exp \left[-\frac{\|\mathbf{r} - \mathbf{s}_{j,m}\|^2}{2\sigma_n^2} \right], \quad (10)$$

and the Euclidean distance metric $D(\mathbf{r}, \mathbf{s}_{j,m})$ is given as:

$$D(\mathbf{r}, \mathbf{s}_{j,m}) = \|\mathbf{r} - \mathbf{s}_{j,m}\|^2. \quad (11)$$

The notation $\|\cdot\|$ denotes the Frobenius norm. This detection process is equivalent to obtaining \hat{m} from $\hat{m} = \arg \max_m \{r_\ell\}_{\ell=1}^L$, and then estimating the index of the SCP from the minimum Euclidean distance metric [7].

System model of other optical SM schemes

The system models for OSSK, GSSK and SPPM are similar to that of GSPPM described above, and they can be obtained by changing some system parameters. Based on the description of each scheme in Section II, a comparison of how the system parameters are defined for each scheme is provided in Table II. The pulse-inversion constants, λ , is employed only in GSPPM, hence it is defined as 1 for all other schemes. Similarly, except for GSSK, a non-return-to-zero pulse pattern is used for the transmitted signal. Consequently, the duty cycle is set to one for OSSK, SPPM, and GSPPM schemes while it varies for GSSK depending on the spatial constellation point of the data symbol.

As an example, a GSPPM scheme can be converted to a GSSK scheme if the signal modulation, i.e. PPM, in GSPPM is removed by setting $L=1$, and the pulse inversion technique

TABLE II: Definition of system parameters for the different OSM schemes

Scheme	K	L	M	T_c	λ
OSSK	N_t	1	$\log_2(N_t)$	T	1
GSSK	2^{N_t}	1	N_t	T	1
SPPM	N_t	L	$\log_2(LN_t)$	T/L	1
GSPPM	2^{N_t}	L	$N_t + \log_2(L)$	T/L	± 1

TABLE III: LED activation and received electrical signal in a GSSK scheme, using 2 LEDs

j	Spatial bits	$\mathbf{v}\mathcal{T}$	Activated LEDs	$y(t)$
1	00	[1, 1]	LEDs 1 & 2	$(1 - \delta)RP_t(h_1 + h_2) + \eta(t)$
2	01	[0, 1]	LED 1	$\delta RP_t h_1 + \eta(t)$
3	10	[1, 0]	LED 2	$\delta RP_t h_2 + \eta(t)$
4	11	[1, 1]	LEDs 1 & 2	$\delta RP_t(h_1 + h_2) + \eta(t)$

is replaced with RZ pulse coding by setting $\{\lambda_j\}_{j=1}^K = 1$ and using the a predefined value for δ as described in Section II. Since $L=1$, then $T_c=T$, which implies that a pulse is transmitted for the entire symbol duration. As an illustration, considering a 2-LED GSSK system, the received signal for all possible GSSK symbols are obtained as shown in Table III. Similarly, the SPPM scheme can be obtained from the GSPPM scheme if only one LEDs is activated during any symbol duration. As such, the LED activation vector, \mathbf{v} , will have only one non-zero entry which will be positioned at the index of the activated LED.

IV. SYNCHRONISATION ERROR ANALYSIS OF GSPPM

Considering a non-ideal system in which the received signal is impaired by errors in timing synchronisation between the LEDs and the receiver, with reference to the receiver clock, such errors introduce timing offset/displacement in the received signal. Due to this offset, some samples of a given data symbol will form part of another data symbol. Hence, the receiver reads a mixture of interfering signals at its sampling instant, which degrades system performance. The theoretical analysis of such effects on the error performance of SM-based OWC systems is provided in this section. Using GSPPM as reference scheme, the probability of symbol error is derived for a GSPPM scheme that is impaired by timing error. The analysis is then extended to study the effect of timing errors on the performance of OSSK, GSSK and SPPM schemes in the next section.

Let $\mathcal{A}_{i,\mu}$ and $\mathcal{A}_{j,m}$ denote two consecutively transmitted symbols, such that $\mathcal{A}_{i,\mu}$ is transmitted in the previous symbol duration, while $\mathcal{A}_{j,m}$ is transmitted in the current symbol duration. If any of the LEDs that are activated to send symbol $\mathcal{A}_{j,m}$ suffers synchronisation issues, then only a portion of the signal energy is included in the MF output for slot m , while the remaining signal energy is spilled over into the next time slot, denoted by m^+ . Let the timing offsets introduced into the signal received from each transmit unit be denoted by $\mathbf{\Delta} = [\Delta_1 \dots \Delta_{\kappa} \dots \Delta_{N_t}]$. Positive time offsets are considered here, but the interpretation also holds for negative offsets. From the expression for the MF output in the absence of noise in (8), the portion of symbol $\mathcal{A}_{j,m}$'s energy that is captured in the MF output for slot m is expressed as:

$$\bar{s}_{j,m}^m = E_c \lambda_j (\mathbf{h} \odot (\hat{\mathbf{1}} - \boldsymbol{\epsilon})) \mathbf{v}_j \quad (12)$$

where the \odot denotes the Hadamard (entry-wise) product, while $\hat{\mathbf{1}}$ represents an $(1 \times N_t)$ unit vector. The vector $\boldsymbol{\epsilon} = [\epsilon_1 \dots \epsilon_{\kappa} \dots \epsilon_{N_t}]$ represents the timing offsets normalised by the pulse (slot) duration T_c , that is, $\epsilon_{\kappa} = \Delta_{\kappa}/T_c$. Similarly, the energy spillover from slot m into the next time slot, m^+ , is given by:

$$\bar{s}_{j,m}^{m^+} = E_c \lambda_j (\mathbf{h} \odot \boldsymbol{\epsilon}) \mathbf{v}_j. \quad (13)$$

Furthermore, if any of the LEDs that are activated to transmit symbol $\mathcal{A}_{i,\mu}$ introduces timing offset in its signal, and the pulse of symbol $\mathcal{A}_{i,\mu}$ is transmitted in its last time slot, that is, $\mu = L$, then the spillover energy from $\mathcal{A}_{i,\mu}$ which is contributed to the MF output in the first slot of $\mathcal{A}_{j,m}$ is given by:

$$\bar{s}_{i,\mu}^{L^+} = E_c \lambda_i (\mathbf{h} \odot \boldsymbol{\epsilon}) \mathbf{v}_i. \quad (14)$$

The effect of the ISI, which results from the energy spillovers described above, depends on the pulse position of both symbols $\mathcal{A}_{i,\mu}$ and $\mathcal{A}_{j,m}$. In the following analysis, by considering all the possible pulse position combinations, we derive the upper bound on the symbol error probability of a GSPPM scheme that is impaired by timing error.

A transmitted symbol is correctly decoded if both the pulse position and the SCP are correctly decoded. Thus, the probability of symbol error is expressed as [7], [15]:

$$P_{c,\text{sym}}^{\text{GSPPM}} = 1 - (P_{c,\text{scp}}^{\text{GSPPM}} \times P_{c,\text{ppm}}^{\text{GSPPM}}) \quad (15)$$

where $P_{c,\text{ppm}}^{\text{GSPPM}} = p(\hat{m} = m)$, is the probability of a correctly decoded pulse position, and $P_{c,\text{scp}}^{\text{GSPPM}} = p(\hat{j} = j | \hat{m} = m)$, is the probability of correctly decoding the SCP given that the pulse position has been correctly decoded. The expressions for $P_{c,\text{scp}}^{\text{GSPPM}}$ and $P_{c,\text{ppm}}^{\text{GSPPM}}$ are derived as follows.

A. Effect of timing offset on the detection of spatial constellation point in GSPPM

For symbol $\mathcal{A}_{j,m}$ which is transmitted by activating the LEDs based on SCP j , the pairwise error probability (PEP) that the receiver decides in favour of SCP k instead of j , is given by:

$$\text{PEP}_m^{j \rightarrow k} = p(D(\bar{\mathbf{r}}, \mathbf{s}_{j,m}) > D(\bar{\mathbf{r}}, \mathbf{s}_{k,m})) \quad (16)$$

where $\bar{\mathbf{r}} = \{\bar{r}_\ell\}_{\ell=1}^L$ is the sampled MF output (in each time slot) which has been impaired by ISI due to timing offset. That is, \bar{r}_ℓ is the sum of the energy of the signal transmitted in slot ℓ , any spillover energy from the preceding slot, and the noise in the receiver, n_ℓ . Using (8) and (11), the distance metrics in (16) can be expressed as:

$$D(\bar{\mathbf{r}}, \mathbf{s}_{j,m}) = \sum_{\substack{\ell=1 \\ \ell \neq m}}^L (n_\ell)^2 + (\bar{r}_m - \lambda_j \mathbf{h} \mathbf{v}_j E_c)^2 \quad (17)$$

Therefore, equation (16) becomes:

$$\text{PEP}_m^{j \rightarrow k} = p((\bar{r}_m - \lambda_j \mathbf{h} \mathbf{v}_j E_c)^2 > (\bar{r}_m - \lambda_k \mathbf{h} \mathbf{v}_k E_c)^2) \quad (18)$$

As mentioned earlier, the value of \bar{r}_m in (18) depends on the position of the transmitted pulses in symbols $\mathcal{A}_{i,\mu}$ and $\mathcal{A}_{j,m}$. For two symbols with L -PPM pulse pattern, there are

$$P_{c,scp}^{GSPPM} \leq 1 - \frac{1}{K} \sum_{j=1}^K \sum_{\substack{k=1 \\ k \neq j}}^K \text{PEP}_m^{j \rightarrow k} = 1 - \frac{1}{KL^2} \sum_{j=1}^K \sum_{\substack{k=1 \\ k \neq j}}^K \left[(L^2 - 1) \text{PEP}_m^{I,j \rightarrow k} + \text{PEP}_m^{II,j \rightarrow k} \right]. \quad (26)$$

L^2 possible pulse position combinations which are grouped under two cases as follows.

Case I: If the pulse position of symbol $\mathcal{A}_{i,\mu}$ is not its last time slot, that is, $1 \leq \mu < L$, or that of symbol $\mathcal{A}_{j,m}$ is not its first time slot, that is, $1 < m \leq L$, then, there is no spillover energy from $\mathcal{A}_{i,\mu}$ into the pulse position of $\mathcal{A}_{j,m}$. Therefore,

$$\begin{aligned} \bar{r}_m &= \bar{s}_{j,m}^m + n_m \\ &= E_c \lambda_j (\mathbf{h} \odot (\hat{\mathbf{1}} - \boldsymbol{\epsilon})) \mathbf{v}_j + n_m, \end{aligned} \quad (19)$$

and the PEP for this case is obtained as:

$$\begin{aligned} \text{PEP}_m^{I,j \rightarrow k} &= p(n(\lambda_k \mathbf{h} \mathbf{v}_k - \lambda_j \mathbf{h} \mathbf{v}_j) > E_c \Omega_I) \\ &= Q\left(\frac{\Omega_I}{|\lambda_k \mathbf{h} \mathbf{v}_k - \lambda_j \mathbf{h} \mathbf{v}_j|} \sqrt{\frac{\gamma_c}{2}}\right) \end{aligned} \quad (20)$$

where

$$\begin{aligned} \Omega_I &= (\lambda_j \mathbf{h} \mathbf{v}_j) [\lambda_j \mathbf{h} \mathbf{v}_j - 2\lambda_j (\mathbf{h} \odot \boldsymbol{\epsilon}) \mathbf{v}_j] \\ &\quad + (\lambda_k \mathbf{h} \mathbf{v}_k) [\lambda_k \mathbf{h} \mathbf{v}_k - 2\lambda_k (\mathbf{h} \odot (\hat{\mathbf{1}} - \boldsymbol{\epsilon})) \mathbf{v}_j], \end{aligned} \quad (21)$$

and the symbol signal-to-noise ratio (SNR) is $\gamma_c = E_c/N_0$. Out of the L^2 possibilities, there are $(L^2 - 1)$ possible combinations of slots μ and m for this case, therefore, the probability of occurrence of this case is $(1 - (1/L^2))$.

Case II: If the pulse position of symbol $\mathcal{A}_{i,\mu}$ is its last time slot, i.e., $\mu = L$, and that of symbol $\mathcal{A}_{j,m}$ is its first time slot, i.e., $m = 1$, then, the spillover energy from $\mathcal{A}_{i,\mu}$ is contributed into the slot m of $\mathcal{A}_{j,m}$. Hence,

$$\begin{aligned} \bar{r}_m &= \bar{s}_{j,m}^m + \bar{s}_{i,\mu}^{L+} + n_m \\ &= E_c [\lambda_j (\mathbf{h} \odot (\hat{\mathbf{1}} - \boldsymbol{\epsilon})) \mathbf{v}_j + \lambda_i (\mathbf{h} \odot \boldsymbol{\epsilon}) \mathbf{v}_i] + n_m. \end{aligned} \quad (22)$$

The probability of occurrence of this case is $1/L^2$, and the PEP is obtained as:

$$\begin{aligned} \text{PEP}_m^{II,j \rightarrow k} &= \frac{1}{K} \sum_{i=1}^K p(n(\lambda_k \mathbf{h} \mathbf{v}_k - \lambda_j \mathbf{h} \mathbf{v}_j) > E_c \Omega_{II}) \\ &= \frac{1}{K} \sum_{i=1}^K Q\left(\frac{\Omega_{II}}{|\lambda_k \mathbf{h} \mathbf{v}_k - \lambda_j \mathbf{h} \mathbf{v}_j|} \sqrt{\frac{\gamma_c}{2}}\right) \end{aligned} \quad (23)$$

where

$$\begin{aligned} \Omega_{II} &= (\lambda_j \mathbf{h} \mathbf{v}_j) [\lambda_j \mathbf{h} \mathbf{v}_j - 2\lambda_j (\mathbf{h} \odot \boldsymbol{\epsilon}) \mathbf{v}_j + 2\lambda_i (\mathbf{h} \odot \boldsymbol{\epsilon}) \mathbf{v}_i] \\ &\quad + (\lambda_k \mathbf{h} \mathbf{v}_k) [\lambda_k \mathbf{h} \mathbf{v}_k - 2\lambda_j (\mathbf{h} \odot (\hat{\mathbf{1}} - \boldsymbol{\epsilon})) \mathbf{v}_j \\ &\quad - 2\lambda_i (\mathbf{h} \odot \boldsymbol{\epsilon}) \mathbf{v}_i]. \end{aligned} \quad (24)$$

Note that the symbol $\mathcal{A}_{i,\mu}$, which is transmitted in the previous symbol duration, can contain any of the K equiprobable SCPs. Hence, $\text{PEP}_m^{II,j \rightarrow k}$ is obtained by taking the average over K equiprobable SCPs, as shown in (23). By combining (20) and (23), the PEP of decoding the SCP is given by:

$$\text{PEP}_m^{j \rightarrow k} = \left(1 - \frac{1}{L^2}\right) \text{PEP}_m^{I,j \rightarrow k} + \frac{1}{L^2} \text{PEP}_m^{II,j \rightarrow k}. \quad (25)$$

For K equally likely SCPs, using the union bound technique [33], the probability of correctly decoding the SCP of the transmitted symbol, conditioned on a correctly decoded pulse position, is given by (26).

B. Effect of timing error on the detection of pulse position in GSPPM

For the transmitted symbol $\mathcal{A}_{j,m}$, the activated LEDs transmit a pulse in slot m of the PPM signal, and the PEP that the receiver decides in favour of slot q instead of slot m is expressed as:

$$\text{PEP}_{m \rightarrow q}^j = p(\mathcal{D}(\bar{\mathbf{r}}, \mathbf{s}_{j,m}) > \mathcal{D}(\bar{\mathbf{r}}, \mathbf{s}_{j,q})) \quad (27)$$

where

$$\mathcal{D}(\bar{\mathbf{r}}, \mathbf{s}_{j,m}) = (\bar{r}_m - s_{j,m})^2 + (\bar{r}_q)^2 \quad (28)$$

The values of \bar{r}_m and \bar{r}_q , and hence $\text{PEP}_{m \rightarrow q}^j$, depend on the position of slot m and q in the PPM signal of symbol $\mathcal{A}_{j,m}$, and on the position of slot μ in the PPM signal of symbol $\mathcal{A}_{i,\mu}$. As in Section IV-A, there are a total L^2 possible pulse-position combinations for symbols $\mathcal{A}_{i,\mu}$ and $\mathcal{A}_{j,m}$, and these combinations are grouped into five different cases. The diagrammatic illustration of these five cases for a 4-PPM pulse pattern is shown in Fig. 5. A summary of the parameters and the expressions for \bar{r}_m and \bar{r}_q for each case is provided in Table IV. These parameters and expressions are used to evaluate (27), and to compute the probability of correctly decoding pulse position as follows.

Case A: For symbol $\mathcal{A}_{i,\mu}$, $1 \leq \mu < L$, and thus, no spillover energy from $\mathcal{A}_{i,\mu}$ is contributed to the MF output in the first slot of $\mathcal{A}_{j,m}$. In symbol $\mathcal{A}_{j,m}$, $1 \leq m < L$, and the energy spillover in $\mathcal{A}_{j,m}$ is from slot m into the adjacent empty slot m^+ . From a total L^2 possible combinations, the probability of occurrence of this case is obtained as:

$$\begin{aligned} \rho_A &= \Pr(1 \leq \mu < L) \times \Pr(1 \leq m < L) \\ &= ((L - 1)/L)^2. \end{aligned} \quad (29)$$

Therefore, using Table IV, the probability of error in decoding the pulse position in this case is:

$$\mathcal{P}_A = \left(\frac{L - 1}{L}\right)^2 \left[\text{PEP}_{m \rightarrow m^+}^j + (L - 2) \text{PEP}_{m \rightarrow q}^j \right] \quad (30)$$

where $\text{PEP}_{m \rightarrow m^+}^j$ is the PEP between slot m and the adjacent slot m^+ , while $\text{PEP}_{m \rightarrow q}^j$, for $\{1 \leq q \leq L, q \neq m, q \neq m^+\}$, is the PEP between slot m and any of the other $(L - 2)$ empty slots in $\mathcal{A}_{j,m}$.

Case B: As in case A above, For symbol $\mathcal{A}_{i,\mu}$, $1 \leq \mu < L$. But, for symbol $\mathcal{A}_{j,m}$, $m = L$. Hence, the energy spillover in $\mathcal{A}_{j,m}$ is from slot m into first time slot of the next symbol. The probability of occurrence of this case is:

$$\rho_B = \Pr(1 \leq \mu < L) \times \Pr(m = L) = (L - 1)/L^2. \quad (31)$$

$$P_{e,\text{sym}}^{\text{GSPPM}} \leq 1 - \left(1 - \frac{1}{K} \sum_{j=1}^K \sum_{\substack{k=1 \\ k \neq j}}^K \text{PEP}_m^{j \rightarrow k} \right) \left(1 - \frac{1}{K} \sum_{j=1}^K (\mathcal{P}_A + \mathcal{P}_B + \mathcal{P}_C + \mathcal{P}_D + \mathcal{P}_E) \right). \quad (40)$$

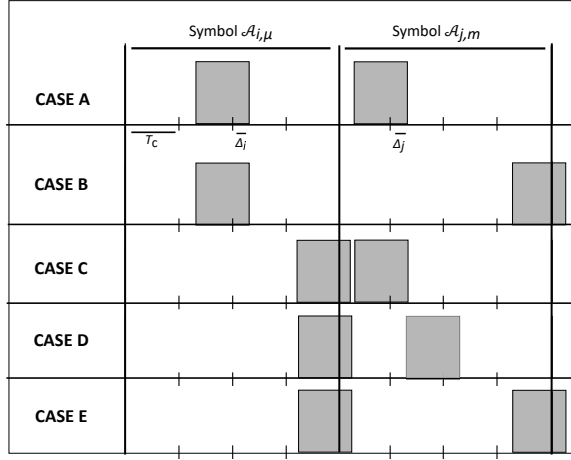


Fig. 5: Illustration of different pulse position combinations for two consecutive symbols $\mathcal{A}_{i,\mu}$ and $\mathcal{A}_{j,m}$, in a GSPPM scheme using 4-PPM. The scalars Δ_i and Δ_j are the timing offsets in the received signal from one of the LEDs activated to send $\mathcal{A}_{i,\mu}$ and $\mathcal{A}_{j,m}$ respectively.

Thus, the probability of error in decoding the pulse position in this case is given by:

$$\mathcal{P}_B = ((L-1)/L^2) \times (L-1) \text{PEP}_{m \rightarrow q}^j \quad (32)$$

where $\text{PEP}_{m \rightarrow q}^j$ for $1 \leq q \leq (L-1)$, is the PEP between slot m and any of the other $(L-1)$ empty slots.

Case C: In this case, the pulse position for symbol $\mathcal{A}_{i,\mu}$ is its last time slot, that is, $\mu = L$, while that of symbol $\mathcal{A}_{j,m}$ is its first time slot, that is, $m = 1$. Hence, any spillover energy from $\mathcal{A}_{i,\mu}$, is contributed to the MF output in slot m of symbol $\mathcal{A}_{j,m}$, while the spillover from slot m in $\mathcal{A}_{j,m}$ is captured in the MF output of the next slot, $m^+ = 2$. The probability of occurrence for this case is given by:

$$\rho_C = \Pr(\mu = L) \times \Pr(m = 1) = 1/L^2, \quad (33)$$

and the probability of error in decoding the pulse position is:

$$\mathcal{P}_C = \frac{1}{KL^2} \sum_{i=1}^K \left[\text{PEP}_{m \rightarrow m^+}^j + (L-2) \text{PEP}_{m \rightarrow q}^j \right] \quad (34)$$

where $\text{PEP}_{m \rightarrow m^+}^j$ is the PEP between slot m and the next slot m^+ , while $\text{PEP}_{m \rightarrow q}^j$, for $3 \leq q \leq L$, is the PEP between slot m and any of the other $(L-2)$ empty slots.

Case D: For symbol $\mathcal{A}_{i,\mu}$, $\mu = L$, while the pulse position of symbol $\mathcal{A}_{j,m}$ is neither its first nor its last time slot, i.e., $1 < m < L$. As a result, any spillover energy from $\mathcal{A}_{i,\mu}$ is contributed to the MF output in the first slot of $\mathcal{A}_{j,m}$, while the spillover from slot m in $\mathcal{A}_{j,m}$ is captured in the MF output of slot m^+ . This case can occur with the probability:

$$\begin{aligned} \rho_D &= \Pr(\mu = L) \times \Pr(2 \leq m < (L-1)) \\ &= (L-2)/L^2. \end{aligned} \quad (35)$$

The probability of error in decoding the pulse position in this case is:

$$\begin{aligned} \mathcal{P}_D &= \frac{(L-2)}{KL^2} \sum_{i=1}^K \left[\text{PEP}_{m \rightarrow 1}^j + \text{PEP}_{m \rightarrow m^+}^j \right. \\ &\quad \left. + (L-3) \text{PEP}_{m \rightarrow q}^j \right] \end{aligned} \quad (36)$$

where $\text{PEP}_{m \rightarrow 1}^j$ is the PEP between slot m and the first slot, $\text{PEP}_{m \rightarrow m^+}^j$ is the PEP between slot m and the adjacent slot m^+ , while $\text{PEP}_{m \rightarrow q}^j$ for $\{2 \leq q \leq L, q \neq m, q \neq m^+\}$, is the PEP between slot m and any of the other $(L-3)$ empty slots.

Case E: For symbol $\mathcal{A}_{i,\mu}$, $\mu = L$, and for symbol $\mathcal{A}_{j,m}$, $m = L$. As a result, while spillover energy from $\mathcal{A}_{i,\mu}$ is contributed to the MF output in the first slot of $\mathcal{A}_{j,m}$, the spillover from slot m in $\mathcal{A}_{j,m}$ is captured in the MF output of the first time slot of the next symbol. This case can occur with the probability:

$$\rho_E = \Pr(\mu = L) \times \Pr(m = L) = 1/L^2, \quad (37)$$

and the probability of error in decoding the pulse position in this case is:

$$\mathcal{P}_E = \frac{1}{KL^2} \sum_{i=1}^K \left[\text{PEP}_{m \rightarrow 1}^j + (L-2) \text{PEP}_{m \rightarrow q}^j \right] \quad (38)$$

where $\text{PEP}_{m \rightarrow 1}^j$ is the PEP between slot m and the first slot, and $\text{PEP}_{m \rightarrow q}^j$ for $1 < q < L$, is the PEP between slot m and any of the other $(L-2)$ empty slots.

The PEP terms in (30), (32), (34), (36) and (38), are obtained by using the corresponding expressions for \bar{r}_m and \bar{r}_q provided in Table IV. The resulting expressions for these PEP terms are shown in Table V. Thus, for K equiprobable SCPs, the probability of correctly decoding the pulse position of the transmitted data symbol is given by:

$$P_{c,\text{ppm}}^{\text{GSPPM}} = 1 - \frac{1}{K} \sum_{j=1}^K (\mathcal{P}_A + \mathcal{P}_B + \mathcal{P}_C + \mathcal{P}_D + \mathcal{P}_E). \quad (39)$$

Combining (26) and (39), the average symbol error probability for a GSPPM scheme impaired by timing synchronisation error is given by (40). Note that for GSPPM scheme, $K=2^{N_t}$. By setting the normalised timing offsets to zero, that is, $\{\epsilon_{\kappa}\}_{\kappa=1}^{N_t} = 0$, the derived expression in (40) reduces to the standard SER expression for a GSPPM scheme without timing errors, as presented in [15, Eq. (26)].

V. EXTENSION OF SYNCHRONISATION ERROR ANALYSIS TO OTHER OPTICAL SM SCHEMES

A. Synchronisation Error Analysis of OSSK

For an OSSK scheme that is affected by timing error in transmitter-receiver synchronisation, the probability of sym-

TABLE IV: Summary of the parameters and expressions for different pulse position combinations in a GSPPM scheme impaired by timing synchronisation error

CASE	Pulse position of symbol $A_{i,\mu}, (\mu)$	Pulse position of symbol $A_{j,m}, (m)$	\bar{r}_m	q	\bar{r}_q
A	$1 \leq \mu < L$	$1 \leq m < L$	$E_c \lambda_j (\mathbf{h} \odot (\hat{\mathbf{1}} - \epsilon)) \mathbf{v}_j + n_m$	m^+ $1 \leq q \leq L$ $q \neq m, q \neq m^+$	$E_c \lambda_j (\mathbf{h} \odot \epsilon) \mathbf{v}_j + n_q$ n_q
B		L	$E_c \lambda_j (\mathbf{h} \odot (\hat{\mathbf{1}} - \epsilon)) \mathbf{v}_j + n_m$	$1 \leq q \leq (L-1)$	n_q
C	L	1	$E_c \lambda_j (\mathbf{h} \odot (\hat{\mathbf{1}} - \epsilon)) \mathbf{v}_j + E_c \lambda_i (\mathbf{h} \odot \epsilon) \mathbf{v}_i + n_m$	m^+ $3 \leq q \leq L$	$E_c \lambda_j (\mathbf{h} \odot \epsilon) \mathbf{v}_j + n_q$ n_q
D		$1 < m < L$	$E_c \lambda_j (\mathbf{h} \odot (\hat{\mathbf{1}} - \epsilon)) \mathbf{v}_j + n_m$	1 m^+ $2 \leq q \leq L$ $q \neq m, q \neq m^+$	$E_c \lambda_i (\mathbf{h} \odot \epsilon) \mathbf{v}_i + n_q$ $E_c \lambda_j (\mathbf{h} \odot \epsilon) \mathbf{v}_j + n_q$ n_q
E		L	$E_c \lambda_j (\mathbf{h} \odot (\hat{\mathbf{1}} - \epsilon)) \mathbf{v}_j + n_m$	1 $1 < q < L$	$E_c \lambda_i (\mathbf{h} \odot \epsilon) \mathbf{v}_i + n_q$ n_q

TABLE V: PEP of pulse position detection for different pulse position combinations in a GSPPM scheme impaired by timing synchronisation error

CASE	q	ρ	PEP $_{m \rightarrow q}^j$
A	m^+	$\left(\frac{L-1}{L}\right)^2$	$Q\left(\sqrt{\gamma_c} \lambda_j (\mathbf{h} \odot (\hat{\mathbf{1}} - 2\epsilon)) \mathbf{v}_j\right)$
	$1 \leq q \leq L, q \neq m, q \neq m^+$		$Q\left(\sqrt{\gamma_c} \lambda_j (\mathbf{h} \odot (\hat{\mathbf{1}} - \epsilon)) \mathbf{v}_j\right)$
B	$1 \leq q \leq (L-1)$	$\frac{L-1}{L^2}$	$Q\left(\sqrt{\gamma_c} \lambda_j (\mathbf{h} \odot (\hat{\mathbf{1}} - \epsilon)) \mathbf{v}_j\right)$
C	m^+	$\frac{1}{L^2}$	$Q\left(\sqrt{\gamma_c} \left[\lambda_j (\mathbf{h} \odot (\hat{\mathbf{1}} - 2\epsilon)) \mathbf{v}_j + \lambda_i (\mathbf{h} \odot \epsilon) \mathbf{v}_i\right]\right)$
	$3 \leq q \leq L$		$Q\left(\sqrt{\gamma_c} \left[\lambda_j (\mathbf{h} \odot (\hat{\mathbf{1}} - \epsilon)) \mathbf{v}_j + \lambda_i (\mathbf{h} \odot \epsilon) \mathbf{v}_i\right]\right)$
D	1	$\frac{(L-2)}{L^2}$	$Q\left(\sqrt{\gamma_c} \left[\lambda_j (\mathbf{h} \odot (\hat{\mathbf{1}} - \epsilon)) \mathbf{v}_j - \lambda_i (\mathbf{h} \odot \epsilon) \mathbf{v}_i\right]\right)$
	m^+		$Q\left(\sqrt{\gamma_c} \left[\lambda_j (\mathbf{h} \odot (\hat{\mathbf{1}} - \epsilon)) \mathbf{v}_j + \lambda_i (\mathbf{h} \odot \epsilon) \mathbf{v}_i\right]\right)$
	$2 \leq q \leq L$ $q \neq m, q \neq m^+$		$Q\left(\sqrt{\gamma_c} \left[\lambda_j (\mathbf{h} \odot (\hat{\mathbf{1}} - 2\epsilon)) \mathbf{v}_j + \lambda_i (\mathbf{h} \odot \epsilon) \mathbf{v}_i\right]\right)$
E	1	$\frac{1}{L^2}$	$Q\left(\sqrt{\gamma_c} \left[\lambda_j (\mathbf{h} \odot (\hat{\mathbf{1}} - \epsilon)) \mathbf{v}_j - \lambda_i (\mathbf{h} \odot \epsilon) \mathbf{v}_i\right]\right)$
	$2 \leq q \leq (L-1)$		$Q\left(\sqrt{\gamma_c} \lambda_j (\mathbf{h} \odot (\hat{\mathbf{1}} - \epsilon)) \mathbf{v}_j\right)$

bol error of the scheme, $P_{e,\text{sym}}^{\text{OSSK}}$, is obtained by using the parameters defined in Table II to modify the derivation in Section IV. First, since signal modulation is not transmitted by the activated LED in OSSK, then $L = 1$. Therefore, all the PEP terms in Table V vanishes, and the error probabilities $\mathcal{P}_A = \dots = \mathcal{P}_E = 0$. Moreover, since the data symbol is encoded solely on the SCP, then the probability of symbol error is equivalent to the probability of error in determining the index of the SCP. By substituting $L=1$, $K=N_t$, $T_c=T$ and $\lambda_i = \lambda_j = \lambda_k = 1, \forall i, j, k$, in (26), the $P_{e,\text{sym}}^{\text{OSSK}}$ is obtained as:

$$P_{e,\text{sym}}^{\text{OSSK}} \leq \frac{1}{N_t} \sum_{j=1}^{N_t} \sum_{\substack{k=1 \\ k \neq j}}^{N_t} \text{PEP}_m^{\text{II},j \rightarrow k} = \frac{1}{(N_t)^2} \sum_{j=1}^{N_t} \sum_{\substack{k=1 \\ k \neq j}}^{N_t} \sum_{i=1}^{N_t} Q\left(\frac{\Omega_{\text{II}}}{|\mathbf{h}\mathbf{v}_k - \mathbf{h}\mathbf{v}_j|} \sqrt{\frac{\gamma_s}{2}}\right) \quad (41)$$

where symbol SNR is $\gamma_s = E_s/N_0$ and energy per symbol $E_s = (RP_t)^2 T$.

Furthermore, since only one LED is activated to transmit the data signal, then the vector \mathbf{v} has only one non-zero element positioned at the index of the SCP, which is equivalent to the index of the activated LED. Hence, the terms in (41) involving

the product of \mathbf{h} and \mathbf{v} can be further simplified. For example, $\mathbf{h}\mathbf{v}_j = h_j$, and $(\mathbf{h} \odot \epsilon) \mathbf{v}_j = h_j \epsilon_j$. Therefore, (41) can be simplified to:

$$P_{e,\text{sym}}^{\text{OSSK}} \leq \frac{1}{(N_t)^2} \sum_{j=1}^{N_t} \sum_{\substack{k=1 \\ k \neq j}}^{N_t} \sum_{i=1}^{N_t} Q\left(\frac{\chi}{|h_k - h_j|} \sqrt{\frac{\gamma_s}{2}}\right) \quad (42)$$

where

$$\chi = h_j^2(1 - 2\tau_j) + 2h_j h_k(\tau_j - 1) + h_k^2 + 2h_i \tau_i (h_j - h_k), \quad (43)$$

and $\tau_\kappa = \Delta_\kappa/T$, for $\kappa=1, \dots, N_t$, is the timing offset normalised by the symbol duration. If the system is perfectly synchronised, then the normalised timing offset associated with each LED becomes zero, that is, $\{\tau_\kappa\}_{\kappa=1}^{N_t} = 0$, and (42) reduces to the standard SER expression for OSSK which can be obtained from [38, Eq. (3)] and [6, Eq. (7)].

B. Synchronisation Error Analysis of GSSK

Without loss of generality, we consider that $\delta=1$ in the following error analysis of GSSK [8], [12]. Since the symbol information is encoded solely on the SCP in GSSK, then the probability of symbol error of GSSK is equivalent to the probability of error in detecting the SCP in a GSPPM scheme. Thus, by substituting $L=1$, $K=2^{N_t}$, and $\lambda_i = \lambda_j = \lambda_k = 1, \forall i, j, k$,

in (26), the symbol error probability of a GSSK scheme impaired by timing error, $P_{e,\text{sym}}^{\text{GSSK}}$, is given by:

$$P_{e,\text{sym}}^{\text{GSSK}} \leq \frac{1}{2^{2N_t}} \sum_{j=1}^{2^{N_t}} \sum_{\substack{k=1 \\ k \neq j}}^{2^{N_t}} \text{PEP}_m^{\text{II},j \rightarrow k} \\ = \frac{1}{2^{2N_t}} \sum_{j=1}^{2^{N_t}} \sum_{\substack{k=1 \\ k \neq j}}^{2^{N_t}} \sum_{i=1}^{2^{N_t}} Q \left(\frac{\mathcal{Z}}{|\mathbf{h}\mathbf{v}_k - \mathbf{h}\mathbf{v}_j|} \sqrt{\frac{\gamma_s}{2}} \right) \quad (44)$$

where

$$\mathcal{Z} = (\lambda_j \mathbf{h}\mathbf{v}_j) [\lambda_j \mathbf{h}\mathbf{v}_j - 2\lambda_j (\mathbf{h} \odot \boldsymbol{\tau}) \mathbf{v}_j + 2\lambda_i (\mathbf{h} \odot \boldsymbol{\tau}) \mathbf{v}_i] \\ + (\lambda_k \mathbf{h}\mathbf{v}_k) [\lambda_k \mathbf{h}\mathbf{v}_k - 2\lambda_j (\mathbf{h} \odot (\hat{\mathbf{1}} - \boldsymbol{\tau})) \mathbf{v}_j \\ - 2\lambda_i (\mathbf{h} \odot \boldsymbol{\tau}) \mathbf{v}_i]. \quad (45)$$

Again, by setting $\{\tau_\kappa\}_{\kappa=1}^{N_t} = 0$, equation (44) reduces to the standard expression for the SER of an optical GSSK scheme without timing errors, as presented in [8, Eq. (15)].

C. Synchronisation Error Analysis of SPPM

The symbol error probability of an SPPM scheme impaired by timing synchronisation error, $P_{e,\text{sym}}^{\text{SPPM}}$, can be obtained by modifying that of the GSPPM scheme presented in Section IV. First, since pulse inversion technique is not used in SPPM, then $\lambda_i = \lambda_j = \lambda_k = 1, \forall i, j, k$. Furthermore, for SPPM, $K = N_t$, and since only one LED is activated to transmit the data signal, then the LED activation vector, \mathbf{v} , has only one non-zero element positioned at the index of the activated LED (as in OSSK). The cases considered in Section IV-A for the detection of SCP in GSPPM also hold for the detection of the transmitter index in SPPM. Hence, from (26), the probability of correctly detecting the LED index (SCP) in SPPM is given by (46).

Similarly, the analysis of pulse position detection in GSPPM provided in Section IV-B also hold for the pulse position detection in SPPM. Therefore, from (39), the probability of correctly decoding the pulse position of the transmitted symbol in SPPM can be written as:

$$P_{c,\text{ppm}}^{\text{SPPM}} = 1 - \frac{1}{N_t} \sum_{j=1}^{N_t} (\mathcal{V}_A + \mathcal{V}_B + \mathcal{V}_C + \mathcal{V}_D + \mathcal{V}_E) \quad (49)$$

where the probabilities $\{\mathcal{V}_A, \dots, \mathcal{V}_E\}$ are provided in Table VI. Combining (46) and (49), the average symbol error probability for an SPPM scheme impaired by timing error is given by:

$$P_{e,\text{sym}}^{\text{SPPM}} \leq 1 - (P_{c,\text{tx}}^{\text{SPPM}} \times P_{c,\text{ppm}}^{\text{SPPM}}). \quad (50)$$

The standard SER expression for an SPPM scheme without timing errors, given in [7, Eq. (23)], can be obtained from the (50) by setting $\{\epsilon_\kappa\}_{\kappa=1}^{N_t} = 0$.

VI. RESULTS AND DISCUSSIONS

In this section, we present the analytical results of the effect of synchronisation error on the four SM schemes studied in the previous sections, and we validate these results with Monte-Carlo simulations. The achieved SER is plotted against the SNR per bit γ_b . The channel path gains are obtained from the simulation of indoor OWC channel using the ray-tracing algorithm reported in [20], [21]. The normalized channel gain values for four transmitters are $\{h_j\}_{j=1}^{N_t} = [1, 0.409, 0.232, 0.143]$.

The error performance plots for OSSK and GSSK schemes (using $N_t = 2$), for five different values of timing offsets, are depicted in Fig. 6 and Fig. 7 respectively. Similar plots for SPPM and GSPPM (using $N_t = 2, L = 2$) are depicted Fig. 8 and Fig. 9 respectively. Note that these results represent the worst-case scenario in which synchronisation error occurs in both transmitters. These results show that the analytical upper bounds in (40), (42), (44), (50) bound the simulation results very tightly. The results also show clearly that synchronisation error has caused performance degradation in the system. For example, at $\text{SER} = 10^{-5}$, compared to the perfectly synchronised case ($\tau = 0$), a timing offset of 10% of the symbol duration results in about 2 dB SNR penalty for OSSK and a about 9 dB SNR penalty for GSSK. Similarly, for SPPM a timing offset of 10% of the slot duration results in SNR penalty of about 3 dB.

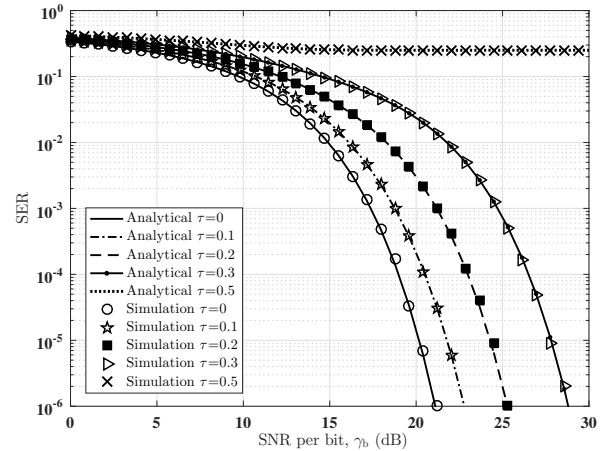


Fig. 6: Error performance of OSSK. $N_t = 2$. Channel gains: $[h_1, h_2] = [1, 0.409]$. Normalised offset: $\tau_1 = \tau_2 = \tau$, $\tau = \Delta/T$.

$$P_{c,\text{tx}}^{\text{SPPM}} = 1 - \frac{1}{N_t L^2} \sum_{j=1}^{N_t} \sum_{\substack{k=1 \\ k \neq j}}^{N_t} \left[(L^2 - 1) Q \left(\frac{\Psi_{\text{I}}}{|h_k - h_j|} \sqrt{\frac{\gamma_c}{2}} \right) + \frac{1}{N_t} \sum_{i=1}^{N_t} Q \left(\frac{\Psi_{\text{II}}}{|h_k - h_j|} \sqrt{\frac{\gamma_c}{2}} \right) \right], \quad (46)$$

$$\Psi_{\text{I}} = h_j^2 (1 - 2\epsilon_j) + 2h_j h_k (\epsilon_j - 1) + h_k^2 \quad (47)$$

$$\Psi_{\text{II}} = h_j^2 (1 - 2\epsilon_j) + 2h_j h_k (\epsilon_j - 1) + h_k^2 + 2h_i \epsilon_i (h_j - h_k). \quad (48)$$

TABLE VI: Probability of error in pulse position detection for different pulse position combinations in SPPM with synchronisation errors.

CASE	Probability of error in decoding the pulse position, \mathcal{V}
A	$\mathcal{V}_A^I = \left(\frac{L-1}{L}\right)^2 \left[Q(h_j(1-2\epsilon_j)\sqrt{\gamma_c}) + (L-2)Q(h_j(1-\epsilon_j)\sqrt{\gamma_c}) \right]$
B	$\mathcal{V}_B^I = \left(\frac{L-1}{L^2}\right) (L-1) Q(h_j(1-\epsilon_j)\sqrt{\gamma_c})$
C	$\mathcal{V}_A^{II} = \frac{1}{N_t L^2} \sum_{i=1}^{N_t} \left[Q((h_j(1-2\epsilon_j) + h_i\epsilon_i)\sqrt{\gamma_c}) + (L-2)Q((h_j(1-\epsilon_j) + h_i\epsilon_i)\sqrt{\gamma_c}) \right]$
D	$\mathcal{V}_B^{II} = \frac{L-2}{N_t L^2} \sum_{i=1}^{N_t} \left[Q((h_j(1-\epsilon_j) - h_i\epsilon_i)\sqrt{\gamma_c}) + Q((h_j(1-\epsilon_j) + h_i\epsilon_i)\sqrt{\gamma_c}) + (L-3)Q((h_j(1-2\epsilon_j) + h_i\epsilon_i)\sqrt{\gamma_c}) \right]$
E	$\mathcal{V}_C^{II} = \frac{1}{N_t L^2} \sum_{i=1}^{N_t} \left[Q((h_j(1-\epsilon_j) - h_i\epsilon_i)\sqrt{\gamma_c}) + (L-2)Q(h_j(1-\epsilon_j)\sqrt{\gamma_c}) \right]$

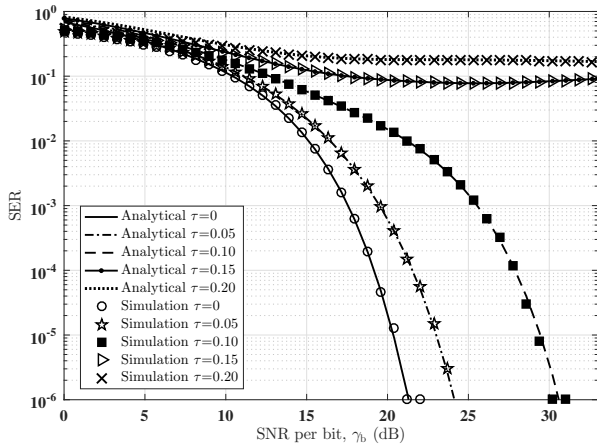


Fig. 7: Error performance of GSSK. $N_t = 2$. Channel gains: $[h_1, h_2] = [1, 0.409]$. Normalised offset: $\tau_1 = \tau_2 = \tau$, $\tau = \Delta/T$.

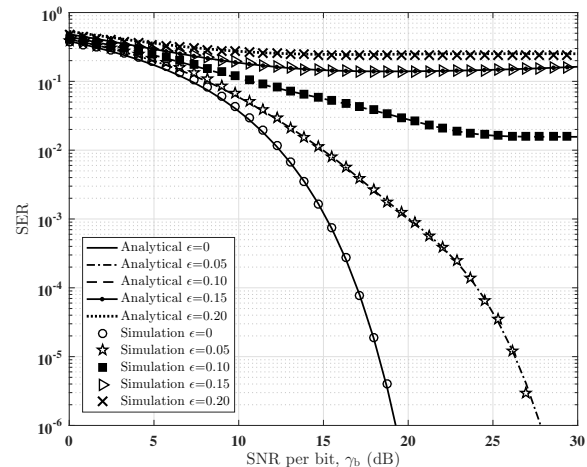


Fig. 9: Error performance of GSPPM. $N_t = 2$, $L = 2$. Channel gains: $[h_1, h_2] = [1, 0.409]$. Normalised offset: $\epsilon_1 = \epsilon_2 = \epsilon$, $\epsilon = \Delta/T_c$.

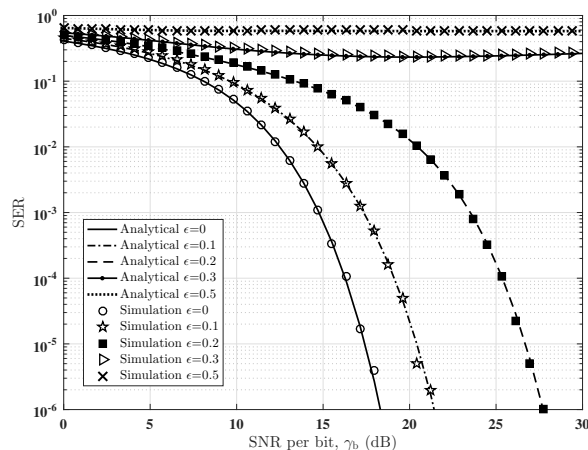


Fig. 8: Error performance of SPPM. $N_t = 2$, $L = 2$. Channel gains: $[h_1, h_2] = [1, 0.409]$. Normalised offset: $\epsilon_1 = \epsilon_2 = \epsilon$, $\epsilon = \Delta/T_c$.

To compare the effect of synchronisation error on the four SM schemes, using $N_t = 2$, $L = 2$, we estimate the achieved SER at $\gamma_b = 20$ dB, for different timing offsets as shown in Fig. 10. For a fair comparison, each modulation scheme is implemented with the same average energy per symbol as the GSPPM scheme, and the timing offset is normalised to the symbol duration. The specified timing offsets are assigned to both transmitters concurrently. It is observed in Fig. 10 that the effect of timing offset is more pronounced in SPPM and GSPPM compared to OSSK and GSSK respectively,

as indicated by the slope the plot for each scheme. The results show a relatively fast increase in SER, as the offset is increased, for SPPM and GSPPM compared to OSSK and GSSK respectively. For example, compared to the zero-offset case ($\Delta = 0$), a timing offset of 10% increases the SER from 10^{-9} to 10^{-2} in SPPM, while the same amount timing offset increases the SER by only a factor of 3 in OSSK. Though SPPM still achieved a better SER compared to OSSK (in the range: $0 \leq \tau \leq 0.09$), the energy efficiency gain that it harnessed from PPM is also rapidly lost to timing offset due to the sensitivity of PPM to synchronisation error [28], [29].

We also note that for $L = 2$, in SPPM and GSPPM, the duration of each PPM time slot is half of the symbol duration, hence, an offset of 10% of the symbol duration represent an offset of 20% of the slot duration and consequently, a 20% spillover in signal energy in SPPM and GSPPM compared to a 10% energy spillover in OSSK and GSSK. In addition, in OSSK and GSSK, timing offset result in intersymbol interference while in SPPM and GSPPM, timing offset can result in both intersymbol interference and intrasymbol interference between PPM time slots. Similarly results and justification exist between GSPPM and GSSK. Furthermore, in Fig. 10, as a result of multiple LEDs activation in GSSK, compared to OSSK with single-LED activation, the effect of timing errors is more significant in GSSK compared to OSSK.

In Fig. 11, we illustrate the impact of channel gain values (transmitter location) on the system performance using the

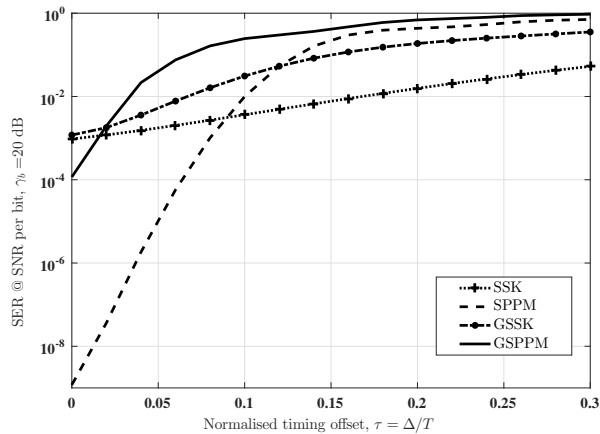


Fig. 10: Comparison of the effect of timing offset on OSSK, SPPM, GSSK and GSPPM. $N_t = 2$, $L = 2$. Channel gains: $[h_1, h_2] = [1, 0.409]$.

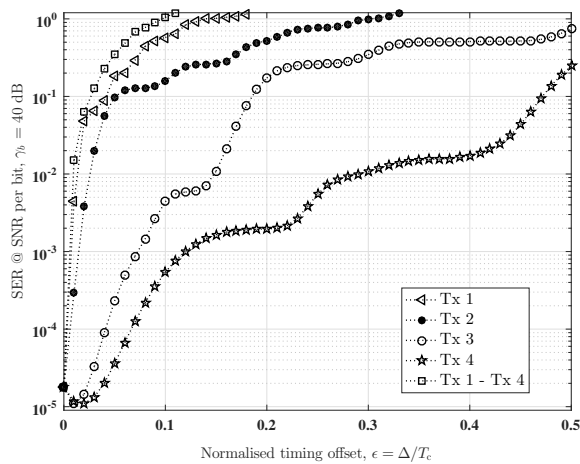


Fig. 11: Impact of channel gain values (transmitter location) on the error performance of GSPPM with timing offsets. $N_t = 4$, $L = 2$. Channel gains: $\{h_i\}_{i=1}^{N_t} = [1, 0.409, 0.232, 0.143]$.

GSPPM scheme as a case study. Using four transmitters, first, we introduce timing offset in one LED and we set the offsets in the other three LEDs to zero. Then, we set equal timing offset in all the four LEDs concurrently. In all the cases, we estimate the achieved SER at $\gamma_b = 40$ dB. Note that the SER values higher than 1 are as result of the union bound used in the analysis. It is observed in Fig. 11 that the lower the channel gain of the transmitter in which synchronisation error occurs, the lesser the impact of the timing offset on the system performance. For instance, a timing offset of 10% of the slot duration, results in an increase in SER from 10^{-5} in the zero-offset case, to an error floor of almost 1 if the offset occurs in transmitter 1 ($h_1 = 1$), and an error floor of 0.2 if the offset occurs in transmitter 2 ($h_2 = 0.409$). While the achieved SER is 4×10^{-3} if the offset occurs in transmitter 3 ($h_3 = 0.232$) and 5×10^{-4} if the offset occurs in transmitter 4 ($h_4 = 0.143$). These results highlights the dependence of the performance of SM technique on the channel gains values of the transmitters.

VII. CONCLUSION

The effect of synchronisation error on optical spatial modulation (SM) technique has been investigated in this paper. As a MIMO technique, SM exploits the physical deployment of multiple transmit and receive elements. Synchronisation error between these multiple elements causes intersymbol interference, thereby increasing symbol error rate (SER). The analytical expressions for SER is derived for four different variants of SM, namely OSSK, GSSK, SPPM and GSPPM, under the condition of imperfect timing synchronisation. These expressions are validated by tightly-matched simulation results, and they provide insight into how error in synchronisation affect the performance of SM techniques. Results show that error performance degrades with increasing synchronisation error.

A comparison of the effect of timing jitter on the performance of the four SM schemes highlights the tolerance of OSSK to small range of synchronisation error compared to GSSK, SPPM, and GSPPM, though the former offers the lowest system capacity. 10% jitter results in an increase in SER by a factor of 3 in OSSK, a factor of 30 in GSSK, 2×10^2 in GSPPM, and 10^7 in SPPM. These results show that accurate synchronisation is critical for optical SM technique, and adding signal modulation to OSSK in order to improve throughput also requires that synchronisation problems must be addressed in order to prevent system performance degradation. Also, we demonstrated the impact of channel gain value (transmitter location) on the system performance using the GSPPM scheme as a case study, and we observe that the lower the channel gain of the transmitter in which synchronisation error occurs, the lesser the impact of the synchronisation error on the system performance. This work has focused on investigating optical SM schemes using pulse modulation methods such as PPM. Considering the benefits of other single-carrier (SC) and multi-carrier (MC) modulation methods such as spectral efficiency and robustness against channel dispersion, in the future, this work will be extended to investigate the effect of synchronisation error on optical SM schemes using SC methods such as QAM, and MC methods such as OFDM.

REFERENCES

- [1] M. Di Renzo, H. Haas, and P. M. Grant, "Spatial modulation for multiple-antenna wireless systems: a survey," *IEEE Communications Magazine*, vol. 49, no. 12, pp. 182–191, 2011.
- [2] T. Fath and H. Haas, "Performance comparison of MIMO techniques for optical wireless communications in indoor environments," *IEEE Transactions on Communications*, vol. 61, no. 2, pp. 733–742, 2013.
- [3] M. Di Renzo, H. Haas, A. Ghayeb, S. Sugiura, and L. Hanzo, "Spatial modulation for generalized MIMO: challenges, opportunities, and implementation," *Proceedings of the IEEE*, vol. 102, no. 1, pp. 56–103, 2014.
- [4] J. Jeganathan, A. Ghayeb, L. Szczecinski, and A. Ceron, "Space shift keying modulation for MIMO channels," *IEEE Transactions on Wireless Communications*, vol. 8, no. 7, pp. 3692–3703, 2009.
- [5] P. Yang, M. Di Renzo, Y. Xiao, S. Li, and L. Hanzo, "Design guidelines for spatial modulation," *IEEE Communications Surveys & Tutorials*, vol. 17, no. 1, pp. 6–26, 2015.
- [6] R. Mesleh, H. Elgala, and H. Haas, "Optical spatial modulation," *Journal of Optical Communications and Networking*, vol. 3, no. 3, pp. 234–244, 2011.
- [7] W. O. Popoola, E. Poves, and H. Haas, "Spatial pulse position modulation for optical communications," *Journal of Lightwave Technology*, vol. 30, no. 18, pp. 2948–2954, 2012.

- [8] —, “Error performance of generalised space shift keying for indoor visible light communications,” *IEEE Transactions on Communications*, vol. 61, no. 5, pp. 1968–1976, 2013.
- [9] P. Yang, Y. Xiao, Y. L. Guan, K. Hari, A. Chockalingam, S. Sugiura, H. Haas, M. Di Renzo, C. Masouros, Z. Liu *et al.*, “Single-carrier SM-MIMO: A promising design for broadband large-scale antenna systems,” *IEEE Communications Surveys & Tutorials*, vol. 18, no. 3, pp. 1687–1716, 2016.
- [10] R. Y. Mesleh, H. Haas, S. Sinanovic, C. W. Ahn, and S. Yun, “Spatial modulation,” *IEEE Transactions on Vehicular Technology*, vol. 57, no. 4, pp. 2228–2241, 2008.
- [11] X. Zhang, S. Dimitrov, S. Sinanovic, and H. Haas, “Optimal power allocation in spatial modulation OFDM for visible light communications,” in *2012 IEEE 75th Vehicular Technology Conference (VTC Spring)*. IEEE, 2012, pp. 1–5.
- [12] W. Popoola, E. Poves, and H. Haas, “Generalised space shift keying for visible light communications,” in *Networks & Digital Signal Processing (CSNDSP), 2012 8th International Symposium on Communication Systems*. IEEE, 2012, pp. 1–4.
- [13] A. Younis, N. Serafimovski, R. Mesleh, and H. Haas, “Generalised spatial modulation,” in *2010 Conference Record of the Forty Fourth Asilomar Conference on Signals, Systems and Computers (ASILOMAR)*. IEEE, 2010, pp. 1498–1502.
- [14] S. Alaka, T. L. Narasimhan, and A. Chockalingam, “Generalized spatial modulation in indoor wireless visible light communication,” in *Global Communications Conference (GLOBECOM), 2015 IEEE*. IEEE, 2015, pp. 1–7.
- [15] H. G. Olanrewaju, J. Thompson, and W. O. Popoola, “Generalized Spatial Pulse Position Modulation for Optical Wireless Communications,” in *2016 IEEE 84th Vehicular Technology Conference (VTC-Fall)*. IEEE, 2016.
- [16] P. M. Butala, H. Elgala, and T. D. Little, “Performance of optical spatial modulation and spatial multiplexing with imaging receiver,” in *Wireless Communications and Networking Conference (WCNC), 2014 IEEE*. IEEE, 2014, pp. 394–399.
- [17] P. F. Mmbaga, J. Thompson, and H. Haas, “Performance Analysis of Indoor Diffuse VLC MIMO Channels Using Angular Diversity Detectors,” *Journal of Lightwave Technology*, vol. 34, no. 4, pp. 1254–1266, Feb 2016.
- [18] J. Zhang, L. Tian, Y. Wang, and M. Liu, “Selection transmitting/maximum ratio combining for timing synchronization of MIMO-OFDM systems,” *IEEE Transactions on Broadcasting*, vol. 60, no. 4, pp. 626–636, 2014.
- [19] A. Saemi, V. Meghdadi, J. Cances, M. Syed, G. Ferre, and J. Dumas, “Fine timing and frequency synchronization for mimo system,” *Proceeding of IST Mobile & Wireless Communications Summit, Dresden, Germany, 2005*.
- [20] J. M. Kahn and J. R. Barry, “Wireless infrared communications,” *Proceedings of the IEEE*, vol. 85, no. 2, pp. 265–298, 1997.
- [21] K. Lee, H. Park, and J. R. Barry, “Indoor Channel Characteristics for Visible Light Communications,” *IEEE Communications Letters*, vol. 15, no. 2, pp. 217–219, 2011.
- [22] Z. Ghassemlooy, W. Popoola, and S. Rajbhandari, *Optical wireless communications: system and channel modelling with Matlab®*. CRC Press, 2012.
- [23] T.-D. Nguyen, O. Berder, and O. Sentieys, “Impact of transmission synchronization error and cooperative reception techniques on the performance of cooperative MIMO systems,” in *IEEE International Conference on Communications, 2008. ICC’08*. IEEE, 2008, pp. 4601–4605.
- [24] S. Jagannathan, H. Aghajan, and A. Goldsmith, “The effect of time synchronization errors on the performance of cooperative MISO systems,” in *IEEE Global Telecommunications Conference Workshops, 2004*. IEEE, 2004, pp. 102–107.
- [25] W. O. Popoola and H. Haas, “Demonstration of the merit and limitation of generalised space shift keying for indoor visible light communications,” *Journal of Lightwave Technology*, vol. 32, no. 10, pp. 1960–1965, 2014.
- [26] L. Zeng, D. C. O’Brien, H. Minh, G. E. Faulkner, K. Lee, D. Jung, Y. Oh, and E. T. Won, “High data rate multiple input multiple output (MIMO) optical wireless communications using white LED lighting,” *IEEE Journal on Selected Areas in Communications*, vol. 27, no. 9, pp. 1654–1662, 2009.
- [27] K. D. Dambul, D. C. O’Brien, and G. Faulkner, “Indoor optical wireless MIMO system with an imaging receiver,” *IEEE photonics technology letters*, vol. 23, no. 2, pp. 97–99, 2011.
- [28] R. M. Gagliardi and S. Karp, *Optical communications*, 2nd ed. Wiley, 1995.
- [29] S. Arnon, “The effect of clock jitter in visible light communication applications,” *Journal of Lightwave Technology*, vol. 30, no. 21, pp. 3434–3439, 2012.
- [30] Y. Fujiwara, “Self-synchronizing pulse position modulation with error tolerance,” *IEEE Transactions on Information Theory*, vol. 59, no. 9, pp. 5352–5362, 2013.
- [31] B. Ghimire, I. Stefan, H. Elgala, and H. Haas, “Time and frequency synchronisation in optical wireless OFDM networks,” in *2011 IEEE 22nd International Symposium on Personal Indoor and Mobile Radio Communications (PIMRC)*. IEEE, 2011, pp. 819–823.
- [32] M. F. G. Medina, O. González, S. Rodríguez, and I. R. Martín, “Timing synchronization for OFDM-based visible light communication system,” in *Wireless Telecommunications Symposium (WTS), 2016*. IEEE, 2016, pp. 1–4.
- [33] J. Proakis and M. Salehi, *Digital communications*, 5th ed. McGraw-Hill, 2008.
- [34] W. O. Popoola, S. Sinanovic, and H. E. Nistazakis, “Enhancing the error performance of optical SSK under correlated channel condition,” in *2016 IEEE International Conference on Communications Workshops (ICC)*. IEEE, 2016, pp. 7–11.
- [35] F. Xu, M.-A. Khalighi, and S. Bourennane, “Impact of different noise sources on the performance of PIN-and APD-based FSO receivers,” in *Proceedings of the 2011, 11th International Conference on Telecommunications (ConTEL)*. IEEE, 2011, pp. 211–218.
- [36] M. A. Khalighi and M. Uysal, “Survey on free space optical communication: A communication theory perspective,” *IEEE Communications Surveys & Tutorials*, vol. 16, no. 4, pp. 2231–2258, 2014.
- [37] E. Bayaki, R. Schober, and R. K. Mallik, “Performance analysis of MIMO free-space optical systems in Gamma-Gamma fading,” *IEEE Transactions on Communications*, vol. 57, no. 11, pp. 3415–3424, 2009.
- [38] T. Fath, M. Di Renzo, and H. Haas, “On the performance of space shift keying for optical wireless communications,” in *2010 IEEE GLOBE-COM Workshops (GC Wkshps)*. IEEE, 2010, pp. 990–994.